The Journal of Experimental Biology 206, 1993-2000

doi:10.1242/jeb.00244

Review

Mitochondria are morphologically heterogeneous within cells

Tony J. Collins* and Martin D. Bootman

Laboratory of Molecular Signalling, The Babraham Institute, Babraham, Cambridge, CB2 4AT, UK

*Author for correspondence (e-mail: tony.collins@bbsrc.ac.uk)

Accepted 15 January 2003

Summary

Mitochondria play key roles in the life and death of cells. We investigated whether mitochondria represent morphologically continuous entities within single intact cells. Physical continuity of mitochondria was determined by three-dimensional reconstruction of fluorescence from mitochondrially targeted DsRed1 or tetra-methyl rhodamine ethyl ester (TMRE). The mitochondria of pancreatic acinar, porcine aortic endothelial (PAE) cells, COS-7 cells and SH-SY5Y cells and neocortical astrocytes all displayed heterogeneous distributions and were of varying sizes. In general, there was a denser aggregation of mitochondria in perinuclear positions than in the cell periphery, where individual isolated mitochondria could clearly be seen. DsRed1 was found to be highly mobile within the matrix of individual mitochondria, with an estimated linear diffusion rate of 1 μm s^{-1}. High-intensity irradiation of subcellular regions bleached the fluorescence of mitochondrially targeted DsRed1, but did not cause the mitochondria to depolarise or fragment. A lack of rapid fluorescence-recovery-after-photobleaching (FRAP) of DsRed1 indicated lumenal discontinuity between mitochondria. We observed a slow (half-time approx. 20 min) recovery of DsRed1 fluorescence within the irradiated area that was attributed to mitochondrial movement or fusion of unbleached and bleached organelles. Mitochondria were not electrically coupled, since typically only individual mitochondria were observed to depolarise following irradiation of TMRE-loaded cells. Our data indicate that the mitochondria within individual cells are morphologically heterogeneous and unconnected, thus allowing them to have distinct functional properties.

Key words: mitochondrial morphology, mitochondrial network, fluorescence-recovery-after-photobleaching (FRAP), tetra-methyl rhodamine ethyl ester (TMRE).

Introduction

Mitochondria have been interesting biologists since the middle of the nineteenth century (for a fascinating review of this history, see Lehninger, 1964). In recent years, mitochondrial research has seen a resurgence due to the recognition of the crucial role played by mitochondria in both apoptosis and calcium (Ca^{2+}) homeostasis. Surprisingly, despite this long history of research, there is yet to be a consensus on the nature of mitochondrial structure – do mitochondria exist as discrete organelles within the cell or is the mitochondrion a single entity more akin to the endoplasmic reticulum (ER)? Since mitochondrial structure is a dynamic balance between fission and fusion, perhaps this question should be rephrased as ‘are mitochondria predominately undergoing fusion to form a network or fission to form discrete organelles?’. Mitochondrial functions, including ATP synthesis, Ca^{2+} homeostasis and apoptosis signalling, could be profoundly affected by whether the mitochondria exist as a continuous network or discrete individuals.

Several lines of evidence have been presented to suggest that mitochondria are physically interconnected and functionally homogenous. Real-time monitoring of mitochondrial membrane potential indicated electrical continuity across large parts of a mitochondrial network in COS-7 cells (De Giorgi et al., 2000), human skin fibroblasts and neonatal rat cardiac myocytes (Amchenkova et al., 1988). However, using the same approach multiple individual mitochondria were observed in adult rat cardiac myocytes (Zorov et al., 2000) and various non-electrically excitable cell types (Collins et al., 2002). Reconstruction of electron micrographs revealed apparent mitochondrial networks in rat hepatocytes (Brandt et al., 1974) and a single large mitochondrion in yeast cells (Hoffman and Avers, 1973); however, the number of mitochondria within yeast cells is thought to vary from one to ten (Koning et al., 1993; Nunnari et al., 1997).

Evidence for the existence of a largely interconnected mitochondrial network in HeLa cells was presented using non-confocal, deconvolution imaging and ‘fluorescence-recovery-after-photobleaching’ (FRAP) (Rizzuto et al., 1998). These authors found that the fluorescence of mitochondrially targeted green fluorescent protein (GFP) recovered after irradiation of

a subcellular region, and suggested that this indicated continuity of the mitochondrial matrix. However, the slow recovery of fluorescence observed by Rizzuto et al. (1998) is not compatible with the rapid translocation of fluorescent proteins within the mitochondrial matrix (Collins et al., 2002; Partikian et al., 1998), and their data are more easily reconciled with the concept of multiple physically discrete mitochondria undergoing infrequent fusion.

Early electron microscopy revealed populations of mitochondria with different matrix densities within single cells (Ord, 1979; Simon et al., 1969), thought to reflect differences in metabolic states (Ord, 1979). In cardiac cells (Jahangir et al., 1999) and skeletal muscle cells (Lombardi et al., 2000; Battersby and Moyes, 1998), two distinct populations of mitochondria are proposed to exist with differing biochemical and respiratory properties. Subcellular heterogeneity in Ca^{2+} sequestration by mitochondria has been reported for pancreatic acinar cells (Park et al., 2001), chromaffin cells (Montero et al., 2002), CHO.T cells (Rutter et al., 1996) and HeLa cells (Collins et al., 2002). Also, asynchronous permeability transition pore opening within single cells has been demonstrated in response to oxidant stress (Collins et al., 2002). These data suggest that mitochondria can behave as functionally discrete entities, consistent with their physical segregation.

The aim of the present study was to compliment previous work (Collins et al., 2002) addressing the connectivity of mitochondria in living mammalian cells, using a range of microscopic techniques. Our conclusions are that, typically, mitochondria exist as lumenally and electrically discontinuous organelles within cells.

Materials and methods

Cell culture and chemicals

Primary cultured HUVEC (human umbilical vein endothelial) cells were obtained from Clonetics (BioWhittaker Inc, Walkersville, MD, USA), cortical astrocytes from P. Cuddon (Babraham Institute), pancreatic acinar cells were kindly provided by Dr P. Thorn (Department of Pharmacology, University of Cambridge, UK), SH-SY5Y neuroblastoma and COS-7 cells by Dr K. Anderson (Babraham Institute) and PAE cells by Dr H. Roderick (Babraham Institute). For HeLa, SH-SY5Y, PAE and COS-7 cells, cell culture was performed as described previously (Bootman et al., 1994).

For imaging studies, the culture medium was replaced with an extracellular medium (EM) containing (mmol l^{-1}): NaCl, 121; KCl, 5.4; $MgCl_2$, 0.8; $CaCl_2$, 1.8; $NaHCO_3$, 6.0; D-glucose, 5.5; Hepes, 25; pH 7.3. All fluorescent dyes were obtained from Molecular Probes (Oregon, USA).

Cells were transfected with mitochondrially targeted DsRed1 (mito-DsRed1) from Clontech (Palo Alto, CA, USA) with Effectene transfection reagent (Qiagen, Crawley, UK), following the manufacturers' recommended protocol.

3-D reconstruction

z-series stacks of mito-DsRed1-expressing and tetra-methyl rhodamine ethyl ester (TMRE)-loaded cells were acquired with a Bio-Rad MRC1024 LSCM (Hemel Hempsted, UK). Subsequent image restoration was achieved with the deconvolution software AutoDeblur (Autoquant, New York, USA) using the 'Power accelerated' blind deconvolution algorithm. Image analysis and processing was performed

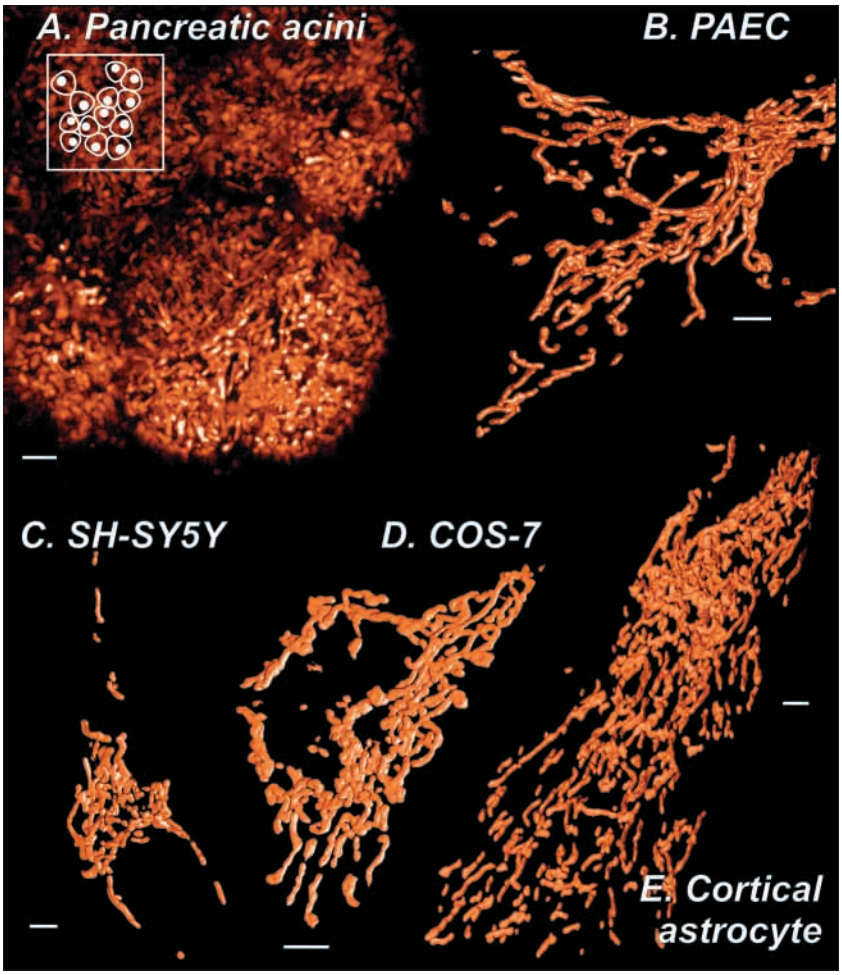

Fig. 1. Morphologically discrete mitochondria in living cells. (A) Volume render of pancreatic acini loaded with the dye TMRE (0.5 μmol l^{-1}, 20 min). The approximate locations of individual acinar cells are outlined in the inset image. Note that this image essentially shows the sub-plasmalemmal mitochondria around the perimeter of the individual acinar cells. (B–E) Surface render of mitochondrially targeted DsRed1-expressing cells. (B) PAE cells, (C) SH-SY5Y cells, (D) COS-7 cells and (E) cortical astrocytes. See text for details. Scale bars, 5 μm.

with the public domain software ImageJ (NIH, http://rsb.info.nih.gov/ij). Single channel surface-rendered images were processed with ImageJ running the VolumeJ plugin (M. Abràmoff; http://www.isi.uu.nl/people/michael/vr.htm).

FRAP

For the FRAP experiments illustrated in Fig. 2, cellular areas of perinuclear mitochondria (typically 25–100 μm^2) were bleached with a Bio-Rad MRC1024 LSCM by briefly digitally zooming into the region of interest with an enhanced laser intensity. The bleaching procedure was continued until the fluorescence intensity of the region being bleached had reached zero. This typically took 5–15 s.

Results

Three-dimensional reconstructions of mitochondrial structure

PAE, cortical astrocytes, SH-SY5Y and COS-7 cells were transfected with DsRed1 targeted to the mitochondrial matrix (mito-DsRed1). For acutely dissociated pancreatic acinar cells that could not be transfected, the mitochondria were specifically visualised with the potentiometric dye TMRE. Attempts to stain pancreatic acinar cell mitochondria specifically using a calcein/cobalt loading protocol (Petronilli et al., 1999) failed as secretory granules retained the calcein (data not shown). Deconvolved confocal *z*-series were either volume-rendered (Fig. 1A) or surface-rendered (Fig. 1B–E) to generate 3-dimensional reconstructions of mitochondria in living cells. In cortical astrocytes, SH-SY5Y, PAE and COS-7 cells, mitochondria were distributed throughout the cell, typically tending to aggregate around the nucleus. Volume reconstruction of pancreatic acini revealed the sub-plasma membrane localisation of mitochondria, as described previously (Park et al., 2001). The sub-plasmalemmal mitochondria were densely concentrated, with little space between individual organelles (Fig. 1A). A less dense distribution of mitochondria was observed deeper inside the pancreatic acinar cells (Fig. 4A), presumably due to their exclusion from the granular and nuclear regions. However, the peri-granular mitochondria that have been shown to prevent Ca^{2+} wave propagation (Tinel et al., 1999) were clearly evident (Fig. 4A).

In all cell types, individual mitochondria were discernible in the periphery of the cell. Both thread-like and grain-like mitochondria were apparent. This differs from primary hepatocytes (Collins et al., 2002) and primary adult ventricular myocytes (Fig. 4D; Zorov et al., 2000), which

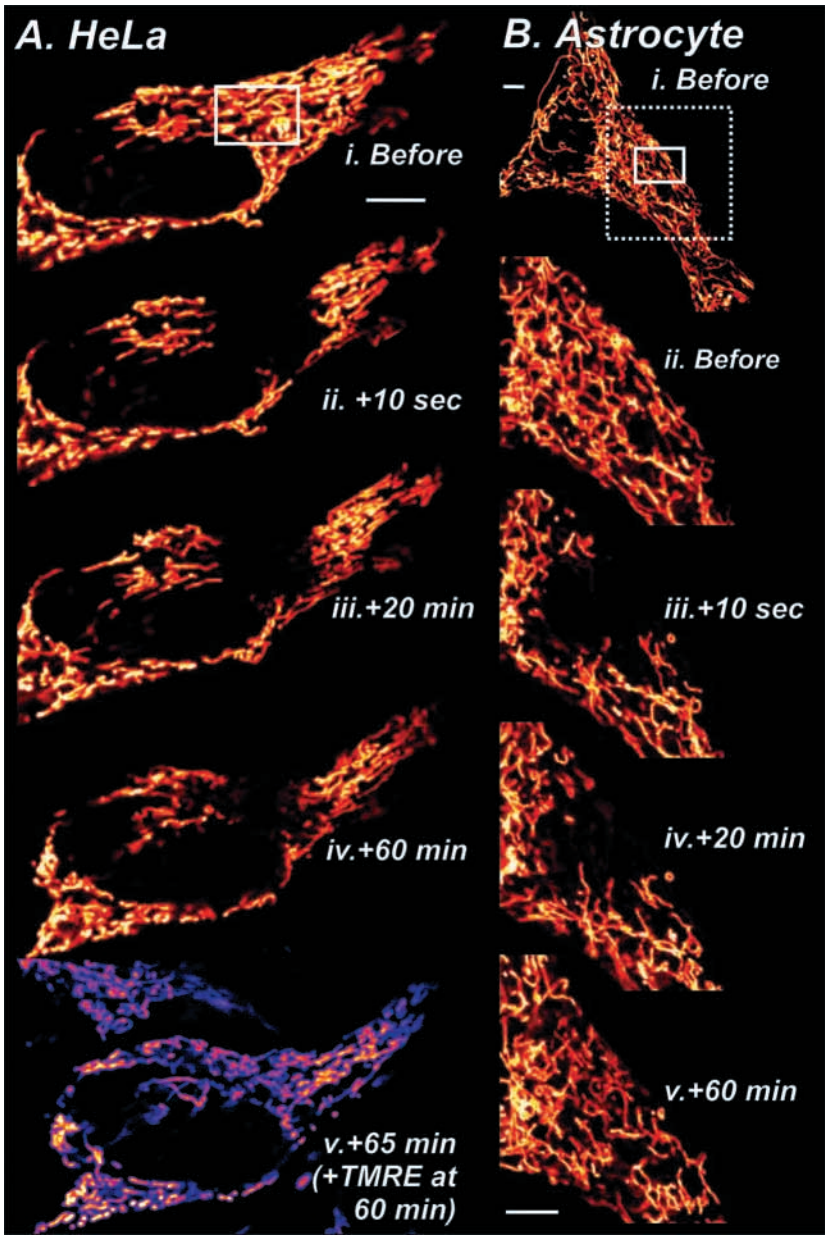

Fig. 2. FRAP analysis of mitochondrial lumenal continuity. (Ai-iv) The DsRed1 fluorescence in a HeLa cell before and 10 s, 20 min and 60 min after photobleaching a small area of mitochondria in the perinuclear aggregation (denoted by white box). (Av) At 60 min post-photobleach, 1 $\mu mol\ l^{-1}$ TMRE was added to the cells for 5 min. The mitochondria that failed to recover DsRed1 fluorescence in Av were stained with TMRE, indicating that their functional integrity was not compromised during laser irradiation. Note that the laser intensity was reduced by 33% in Av compared to Ai-iv, to prevent reactive oxygen species (ROS) production and permeability transition pore (PTP) opening. See text for details. (Bi-v) The DsRed1 fluorescence in a cortical astrocyte before and 10 s, 20 min and 60 min after photobleaching the area denoted by the white box in Bi. (Bii–v) The region of the cell bounded by the broken line in A on an expanded scale. Scale bars, 5 μm.

seem to have predominantly, if not exclusively, grain-like mitochondria.

FRAP of fluorophores in the mitochondrial matrix

Whilst individual mitochondria were clearly visible in the periphery of cells, it was less clear whether the mitochondria in the perinuclear region were continuous or only densely aggregated. To probe this we used the technique of FRAP, which involved bleaching mitochondrially targeted DsRed1 in a subcellular region using brief high-intensity illumination with the confocal zoom increased. The bleaching procedure was continued until fluorescence in the bleached area was reduced to zero. Any subsequent recovery of fluorescence in the bleached region occurs due to inward diffusion of unbleached fluorophore molecules. In HeLa cells (Fig. 2A), the fluorescence failed to significantly recover in the centre of the photobleached area for up 1 h post irradiation. The bleached mitochondria were still intact and functional since they loaded with TMRE, a membrane potential-sensitive indicator, demonstrating that they were still polarised (Fig. 2Av). DsRed1 fluorescence recovered slightly more rapidly in cortical astrocytes, where 5% and 60% of the original fluorescence recovered after 20 min and 1 h, respectively (Fig. 2B).

A critical control for the FRAP experiments is the demonstration that the fluorophore is sufficiently mobile to have reached the bleached cellular areas during the recovery phase. We therefore examined the rate of diffusion of DsRed1 within the mitochondrial matrix. The end portion of a clearly distinct long mitochondrion (Fig. 3A, arrowhead) was photobleached using the same protocol described earlier. Following irradiation, the rate of fluorescence recovery along the mitochondrion was measured and a linear diffusion rate for DsRed1 was estimated at approximately 1 $\mu m\ s^{-1}$ (Fig. 3). DsRed1 therefore has a rapid mobility within the mitochondrial matrix.

These data indicate that if mitochondria form a lumenally interconnected network, DsRed1 can diffuse sufficiently fast for FRAP to be apparent within a few minutes following photobleaching. In all the cells we have tested (Fig. 2; Collins et al., 2002), irradiation of a subcellular region that wholly encompassed several mitochondria caused a bleach that persisted for at least several tens of minutes. This indicates a lack of mitochondrial lumenal connectivity. This slow recovery of fluorescence in such bleached subcellular regions is due to organelle movement or fusion of unbleached and bleached mitochondria, rather than to diffusion of DsRed1 along interconnected mitochondria.

Mitochondria are electrically discontinuous

The electrical continuity of mitochondria was determined using the phenomenon of irradiation-induced depolarisation. The combination of high mitochondrial concentrations of TMRE (1 $\mu mol\ l^{-1}$ for 20 min), plus moderate to high laser irradiation during confocal imaging, results in the rapid depolarisation of mitochondria. This is thought to be due to the generation of reactive oxygen species (ROS) that trigger the mitochondrial permeability transition pore (PTP). In many cases, PTP occurs initially as transient stochastic events, usually followed by a permanent opening. Mitochondria that are electrically continuous show synchronous depolarisations.

In HeLa cells, HUVEC cells, pancreatic acinar cells and adult ventricular myocytes, depolarisation of individual electrically discrete mitochondria was clearly visible (Fig. 4). The TMRE fluorescence in individual mitochondria usually flickered several times, indicative of transient PTP events. Eventually, the TMRE fluorescence was lost from individual mitochondria, presumably when an irreversible opening of the PTP occurred. The flickering and loss of TMRE florescence was randomly observed throughout the mitochondrial population of individual cells.

With HeLa cells and ventricular myocytes, the majority of mitochondria displayed transient PTP events. Within pancreatic acinar cells, rapid depolarisations were obvious in a subset of the mitochondria. A significant number showed no electrical activity, and the TMRE fluorescence in these

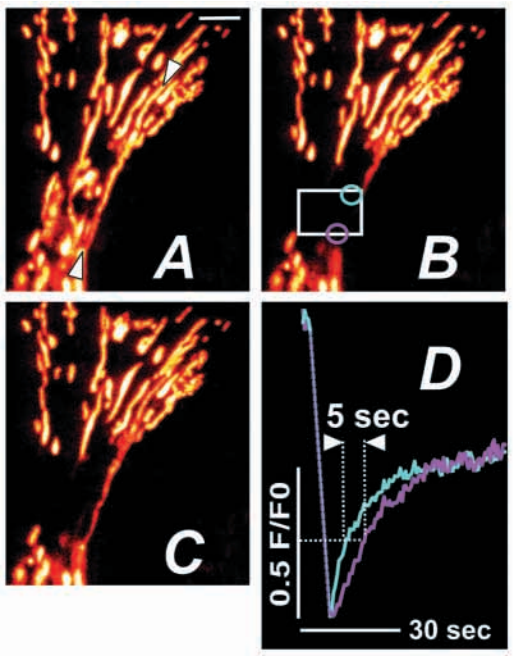

Fig. 3. Rapid mobility of DsRed1 within the mitochondrial matrix. A long mitochondrion in the periphery of a HeLa cell was located (A, arrowheads). A small area at one end of the mitochondrion (B, white square) was photo-bleached. (C) The fluorescence recovery was monitored for 90 s at 2 Hz. Fluorescence from a region at the photo-bleached end of the mitochondria (blue circle in 3B and corresponding blue line in D) was compared with the fluorescence from a region that was also photo-bleached but 5 μm closer to the unbleached end of the mitochondria (purple circle in 3B and corresponding purple line in D). The half-maximum fluorescence recovery (0.5 F/F_0) took 5 s longer in the site 5 μm further from the unbleached end of the mitochondrion, giving an estimated linear diffusion rate for DsRed1 of approximately 1 $\mu m\ s^{-1}$ along the mitochondrion. Scale bar, 5 μm.

organelles was lost due a progressive bleach of the indicator (Fig. 4Aii).

Atypical interconnected mitochondrial networks

The data presented above and in our previous study (Collins et al., 2002), clearly establish that mitochondria are lumenally and electrically discontinuous in several primary cell types and cell lines. In a very few instances, however, we have observed cells that seemed to posses a single large interconnected mitochondrion (Fig. 5). Having visualised mitochondria in many thousands of cells of many different types, we have so far seen only three individual cells (one HeLa, one cortical astrocyte and one HUVEC cell) displaying an interconnected mitochondrion. This phenotype is striking and is readily identifiable in cells expressing mitochondrial-specific fluorophores. In each situation where cells with an interconnected mitochondrion were observed, it was atypical in that all the surrounding cells had clearly discontinuous mitochondria. We would estimate that the frequency of cells bearing an interconnected mitochondrion is significantly less than 0.1%. Although they are extremely rare, the instances of cells with interconnected mitochondria provide a situation where we could examine whether mitochondria can behave as electrically continuous entities, and if DsRed1 can diffuse throughout a large mitochondrial matrix.

We examined the electrical continuity of the apparently interconnected mitochondrion in the HUVEC cell using the TMRE- and laser-induced PTP activation protocol described above. Essentially, we observed that the majority of the mitochondrial network flickered simultaneously throughout the cell (Fig. 5A). Note the dramatic decline in fluorescence in Fig. 5Aii and its recovery to the previous level 8 s later in Fig. 5Aiii. Eventually, after three of these depolarisation and recovery events, the TMRE fluorescence was lost following an irreversible PTP opening. Although this cell appeared to possess a largely interconnected mitochondrion, there were also a few smaller mitochondria that retained TMRE fluorescence after the large mitochondrion had irreversibly depolarised (Fig. 5Aiv).

The cortical astrocyte possessing the interconnected mitochondrion was used to examine the movement of DsRed1 within the mitochondrial matrix. Photobleaching a small region of the cell (Fig. 5Bi,ii) reduced the mitochondrial DsRed1 fluorescence within that area to negligible levels. Within 10 s of the irradiation, the fluorescence had visibly recovered within the bleached area (Fig. 5Biii), and after 2 min the fluorescence had fully recovered (Fig. Biv). Simultaneous with the recovery of fluorescence in the bleached area, the DsRed1 emission

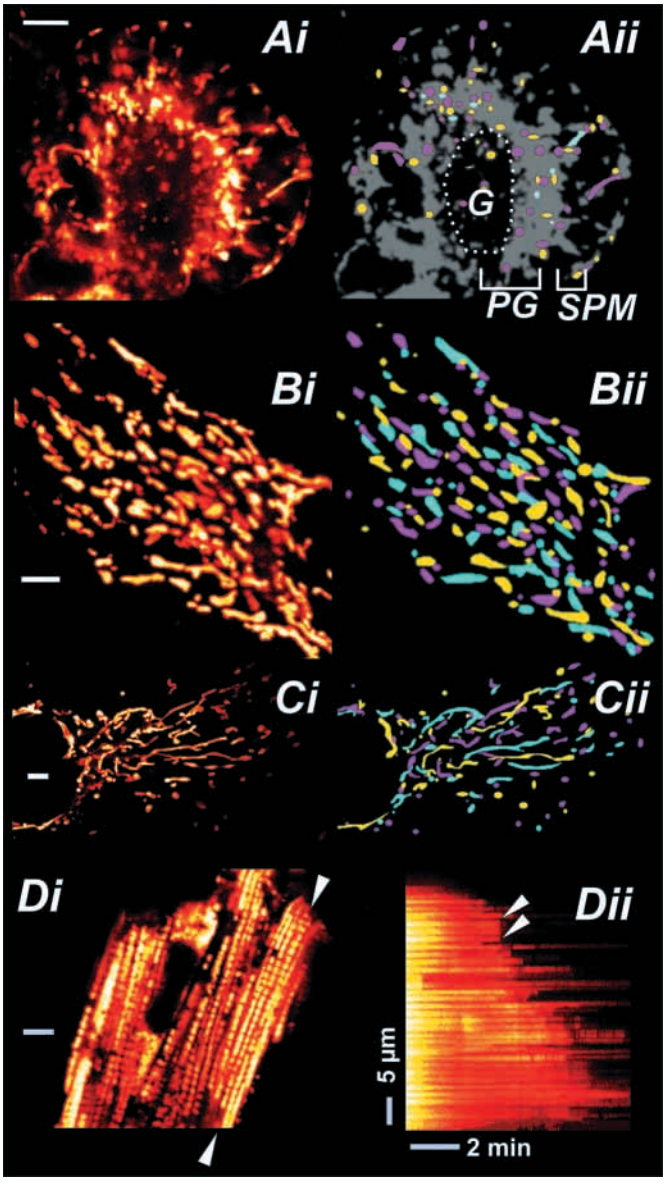

Fig. 4. Electrical discontinuity of mitochondria, demonstrated by asynchronous depolarisation events induced by TMRE plus laser irradiation. Cells were loaded with TMRE and imaged with a moderate laser intensity (30 µW at objective). Rapid mitochondrial depolarisation events appeared as loss of fluorescence between frames (typically 2–4 s). (A) A TMRE-loaded pancreatic acinar cell. Please note that the image is a median section of a cell where the apical region would project out of the figure and the basal pole behind the figure. The locations of mitochondria that showed clear depolarisation events are mapped in (Aii). The grey areas denote TMRE-stained mitochondria that did not flicker. G, the position of the granular region, which is bounded by the perigranular mitochondria (PG). The subplasmalemmal (SPM) mitochondria can been seen around the outside of the cell. (Bi–Di) Portions of a HeLa cell (Bi), HUVEC cells (Ci) and ventricular cardiomyocyte (Di), following loading with TMRE. (Bii–Dii) The positions of electrically discrete mitochondria are depicted in the HeLa cell (Bii) and HUVEC cell (Cii). The maps of individual electrically isolated mitochondria were constructed by monitoring the locations of individual depolarisation events over time. The magenta, cyan and yellow colouration is used to indicate the positions of the electrically isolated mitochondria, and does not indicate any relationships between the organelles. (Dii) A line-scan plot derived from the region between the arrowheads in (Di), illustrating the asynchronous flickering of the majority of mitochondria. A few mitochondria do appear to depolarise synchronously (Dii, arrowheads). Scale bars, 5 µm.

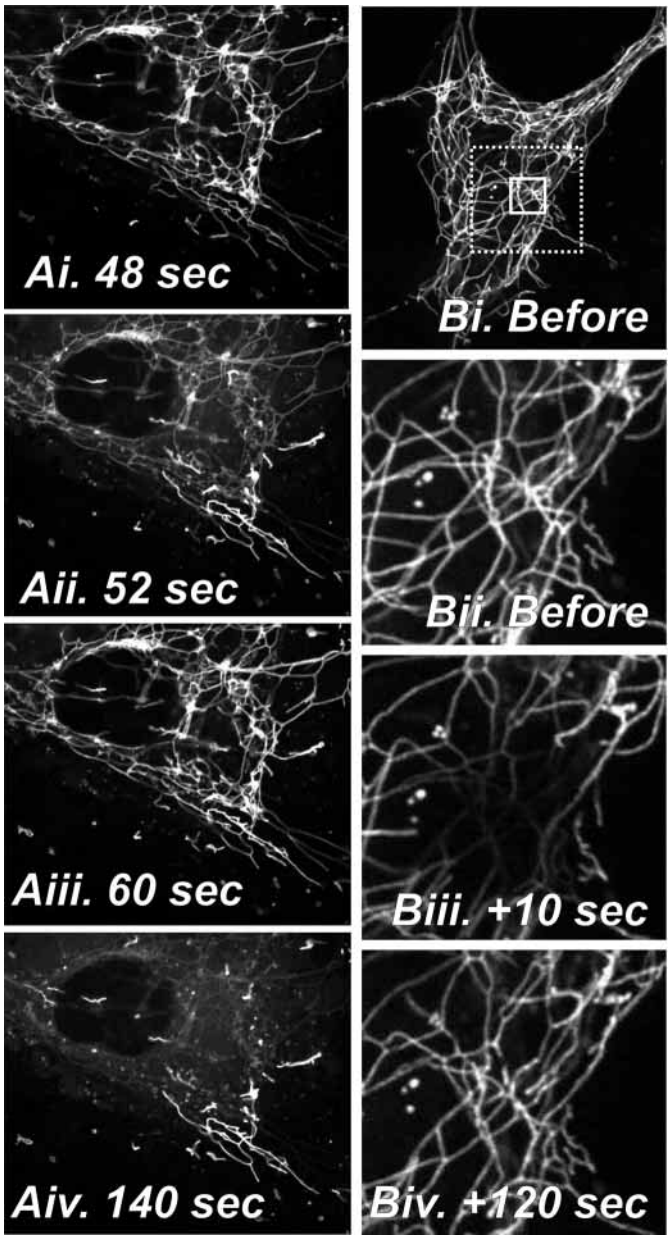

Fig. 5. Examples of atypical interconnected mitochondrial networks. (A) HUVEC cell loaded with TMRE was imaged with moderate laser intensity to trigger depolarisation of mitochondria by spontaneous PTP activation. This unusual HUVEC cell showed synchronous depolarisation across a large mitochondrial network. At 48 s (Ai) the mitochondria in the cell are all polarised, at 52 s (Aii) a large electrically continuous area was seen to depolarise, and 8 s later (Aiii) it had repolarised. After 120 s (Aiv) of imaging, this large electrically continuous mitochondrion depolarised again and did not recover during the experiment (5 min). (B) A cortical astrocyte that was found to have lumenally continuous mitochondria using FRAP. (Bii–iv) The region of the cell bounded by the dashed box in Bi on an expanded scale. The cell was imaged before (Bi,ii), approximately 10 s (Biii) and 120 s after (Biv) after bleaching a small area of the mitochondrion (the bleached region is denoted by the solid white box). During the photobleach process, the laser intensity was increased and sufficient irradiation was applied to reduce the fluorescence in the bleached area to zero. Despite this complete bleach, the fluorescence can already be seen to have partially recovered 10 s later and fully equilibrated after 120 s (Biv). Scale bar, 5 μm.

declined in the other portions of the interconnected mitochondrion, until equilibrium was established.

Discussion

Using 3-dimensional reconstruction, FRAP and measurement of electrical continuity, we have investigated the structure of mitochondria in living mammalian cells. As reported previously (Collins et al., 2002), the typical phenotype is a morphologically and functionally heterogeneous mitochondrial population.

Individual mitochondria can be clearly seen in the three-dimensional reconstructions shown in Fig. 1. Physically isolated mitochondria are easiest to see in the periphery of cells, where they are usually sparsely arranged. The exception to this is pancreatic acinar cells, where a dense uninterrupted layer of mitochondria was found beneath the plasma membrane. Even in the case of pancreatic acinar cells, however, individual mitochondria are visible. The dense perinuclear aggregates of mitochondria in PAE cells, SH-SY5Y cells, COS-7 cells and cortical astrocytes appear as a lumenally continuous network, due to the inability to see the ends of individual organelles. However, when the lumenal continuity of this aggregation was tested using the FRAP technique, it was found to be discontinuous (Fig. 2).

The slow recovery of DsRed1 fluorescence following photobleaching of subcellular areas in HeLa cells and astrocytes (Fig. 2) contrasts with rapid diffusion of this fluorophore within the mitochondrial matrix (Figs 3, 5B). We therefore consider that the slow recovery of fluorescence is not due to lumenal tunnelling of DsRed1, but rather to movement of mitochondria or fusion of unbleached to bleached mitochondria. Interestingly, astrocytes and HeLa cells differed significantly in their slow recovery from photobleaching (Fig. 2), possibly reflecting different mitochondrial fusion rates in these cell types. Our empirical observations also suggest that HeLa cell mitochondria appeared to be less mobile than astrocyte mitochondria (data not shown). Since DsRed1 is can diffuse quickly within the mitochondrial matrix (Fig. 3), a lumenally continuous mitochondrial network would have recovered within 2 min (Fig. 5B). Our measured rate of diffusion of DsRed1 within the mitochondrial matrix (approx. 1 $\mu m\ s^{-1}$) is comparable to that of EGFP within the ER and mitochondrial matrixes (Partikian et al., 1998; Subramanian and Meyer, 1997).

As previously reported, the mitochondria in HeLa cells (Collins et al., 2002) and adult cardiac myocytes (Zorov et al., 2000) were found to be electrically discontinuous (Fig. 4B,C). In adult cardiac myocytes the mitochondrial depolarisation events, whilst asynchronous, seemed to occur in a wave across

the cell (Fig. 4Dii). This wave was too slow to represent electrical continuity, which rapidly spreads between interconnected mitochondria (see Fig. 5) and is consistent with a diffusable messenger being released upon mitochondrial depolarisation acting to trigger depolarisation in neighbouring mitochondria. We have also seen a similar phenomenon in primary rat hepatocytes (C.T.J. and M.D.B., unpublished data). Most likely, the diffusable messenger is a ROS, released upon PTP opening (Zorov et al., 2000). These ROS act upon neighbouring mitochondria, already under ROS stress from TMRE irradiation, precipitating PTP opening and generation of more ROS. The wave of depolarisation therefore represents successive PTP induction and ROS-induced ROS release (Zorov et al., 2000).

In a detailed study of Ca^{2+} sequestration by mitochondria in pancreatic acinar cells, it was demonstrated that the mitochondria are segregated in three regions: sub-plasmalemmal, perigranular and perinuclear (Park et al., 2001). We have also visualised such sub-plasmalemmal (Fig. 1A) and perigranular (Fig. 4Ai) mitochondria. Rings of perinuclear mitochondria were not as obvious since we did not specifically determine the location of nuclei. The study by Park et al. (2001) demonstrated the lack of Ca^{2+} tunnelling between the mitochondria in an individual acinar cell. We now report that the mitochondria within pancreatic acinar cells are also electrically discontinuous (Fig. 4A). These data, therefore, strongly support the hypothesis that pancreatic acinar cells have morphologically and functionally discrete mitochondria. The perigranular mitochondria form a dense aggregation between the apical and basal poles of the acinar cells and have been shown to limit the spread of Ca^{2+} waves inside hormone-stimulated cells (Tinel et al., 1999). The sub-plasmalemmal mitochondria also form a dense sheet of mitochondria that extends completely around the cells (Figs 1A, 4A1). These mitochondria may have significant roles in controlling functions of the basal membrane in acinar cells.

There is a striking difference in the distribution of mitochondria in pancreatic acinar cells compared to the other cell types studied here. In most cell types, mitochondria are found to be most densely aggregated in the cell centre (Fig. 1) where they are often intertwined with the most concentrated strands of the endoplasmic reticulum (Collins et al., 2002) or regularly spaced around myofibrils and the sarcoplasmic reticulum in the case of striated muscle (Fig. 4D). However, in pancreatic acinar cells, the mitochondria appear to be sparse in the basal region where the nucleus and rough endoplasmic reticulum is located. In a sense, pancreatic acinar cell mitochondria appear to be largely excluded from regions where other organelles are densely packed.

Very rarely, we have observed cells possessing mitochondria that seemingly formed a continuous network. These cells were immediately obvious, with very few mitochondrial 'ends' visible (Fig. 5). These may be cells in which the mitochondrial fission/fusion machinery has shifted its balance towards fusion. The mitochondrial structure in these cells is reminiscent of COS-7 cells expressing the dominant negative mutated Drp1 protein, Drp1-K38A, and the mitofusin protein, Mfn2 (Santel and Fuller, 2001). In these cells, fission is inhibited by Drp1-K38A and fusion promoted by Mfn2. The infrequency of cells with an interconnected mitochondrion suggest to us that this phenotype is not representative of a stage in the cell cycle, as in our asynchronous cultures we would expect a higher percentage to show such morphology. Similarly, in a homogenous culture we would rule out a response to an environmental signal.

Fission and fusion of mitochondria over the lifetime of a cell means that in certain respects mitochondria will effectively act as a single continuous network. This appears to be the case with lumenal proteins (Nunnari et al., 1997). Describing mitochondria as a single continuous network, however, likens them to the ER, which is also a dynamic organelle constantly undergoing fission and fusion (Lee and Chen, 1988), but unlike mitochondria, the ER is a demonstrably continuous organelle (C.T.J. and M.D.B., unpublished data; Subramanian and Meyer, 1997; Terasaki et al., 1994), at least for the majority of interphase cells. Clearly, mitochondria vary substantially in their morphology and distribution between different cell types. Despite such differences, it is obvious that unless perturbed, the balance lies in favour of fission into morphologically and functionally distinct entities.

We thank *The Journal of Experimental Biology* for its kind invitation to present this work. This work was supported by the BBSRC. M.D.B. gratefully acknowledges the support of a Royal Society University Research Fellowship.

References

Amchenkova, A. A., Bakeeva, L. E., Chenksov, Y. S., Skulachev, V. P. and Zorov, D. B. (1988). Coupling membranes as energy-transmitting cables. 1. Filamentous mitochondria in fibroblasts and mitochondrial clusters in cardiomyocytes. *J. Cell Biol.* **107**, 481-495.

Battersby, B. J. and Moyes, C. D. (1998). Are there distinct subcellular populations of mitochondria in rainbow trout red muscle? *J. Exp. Biol.* **201**, 2455-2460.

Bootman, M. D., Cheek, T. R., Moreton, R. B., Bennett, D. L. and Berridge, M. J. (1994). Smoothly graded Ca^{2+} release from inositol 1,4,5-trisphosphate-sensitive Ca^{2+} stores. *J. Biol. Chem.* **269**, 24783-24791.

Brandt, J. T., Martin, A. P., Lucas, F. V. and Vorbeck, M. L. (1974). The structure of rat liver mitochondria: a reevaluation. *Biochem. Biophys. Res. Commun.* **59**, 1097-1103.

Collins, T. J., Berridge, M. J., Lipp, P. and Bootman, M. D. (2002). Mitochondria are morphologically and functionally heterogeneous within cells. *EMBO J.* **21**, 1616-1627.

De Giorgi, F., Lartigue, L. and Ichas, F. (2000). Electrical coupling and plasticity of the mitochondrial network. *Cell Calcium* **28**, 365-370.

Hoffman, H. P. and Avers, C. J. (1973). Mitochondrion of yeast: ultrastructural evidence for one giant, branched organelle per cell. *Science* **181**, 749-751.

Jahangir, A., Holmuhamedov, E. L. and Terzic, A. (1999). Two mitochondrial populations in the heart: Are subsarcolemmal mitochondria the primary target of mitochondrial K-ATP channel opener action? *Circulation* **100**, 1798.

Koning, A. J., Lum, P. Y., Williams, J. M. and Wright, R. (1993). $DiOC_6$ staining reveals organelle structure and dynamics in living yeast-cells. *Cell Motil. Cytoskel.* **25**, 111-128.

Lee, C. and Chen, L. B. (1988). Dynamic behaviour of endoplasmic-reticulum in living cells. *Cell* **54**, 37-46.

Lehninger, A. L. (1964). *The Mitochondrion: Molecular Basis of Structure and Function.* W.A. Benjamin, Inc., New York

Lombardi, A., Damon, M., Vincent, A., Goglia, F. and Herpin, P. (2000).

Characterisation of oxidative phosphorylation in skeletal muscle mitochondria subpopulations in pig: a study using top-down elasticity analysis. *FEBS Lett.* **475**, 84-88.

Montero, M., Alonso, M. T., Albillos, A., Cuchillo-Ibanez, I., Olivares, R., Villiotou, V. and Alvarez, J. (2002). Effect of inositol 1,4,5-trisphosphate receptor stimulation on mitochondrial [Ca^{2+}] and secretion in chromaffin cells. *Biochem. J.* **365**, 451-459.

Nunnari, J., Marshall, W. F., Straight, A., Murray, A., Sedat, J. W. and Walter, P. (1997). Mitochondrial transmission during mating in *Saccharomyces cerevisiae* is determined by mitochondrial fusion and fission and the intramitochondrial segregation of mitochondrial DNA. *Mol. Biol. Cell* **8**, 1233-1242.

Ord, M. J. (1979). The effect of chemicals and radiations within the cell: An ultrastructural and micrurgical study using *Amoeba proteus* as a single-cell model. *Int. Rev. Cytol.* **61**, 229-281.

Park, M. K., Ashby, M. C., Erdemli, G., Petersen, O. H. and Tepikin, A. V. (2001). Perinuclear, perigranular and sub-plasmalemmal mitochondria have distinct functions in the regulation of cellular calcium transport. *EMBO J.* **20**, 1863-1874.

Partikian, A., Olveczky, B., Swaminathan, R., Li, Y. and Verkman, A. S. (1998). Rapid Diffusion of Green Fluorescent Protein in the Mitochondrial Matrix. *J. Cell Biol.* **140**, 821-829.

Petronilli, V., Miotto, G., Canton, M., Brini, M., Colonna, R., Bernardi, P. and Di Lisa, F. (1999). Transient and long-lasting openings of the mitochondrial permeability transition pore can be monitored directly in intact cells by changes in mitochondrial calcein fluorescence. *Biophys. J.* **76**, 725-734.

Rizzuto, R., Pinton, P., Carrington, W., Fay, F. S., Fogarty, K. E., Lifshitz, L. M., Tuft, R. A. and Pozzan, T. (1998). Close contacts with the endoplasmic reticulum as determinants of mitochondrial Ca^{2+} responses. *Science* **280**, 1763-1766.

Rutter, G. A., Burnett, P., Rizzuto, R., Brini, M., Murgia, M., Pozzan, T., Tavare, J. M. and Denton, R. M. (1996). Subcellular imaging of intramitochondrial Ca^{2+} with recombinant targeted aequorin – significance for the regulation of pyruvate-dehydrogenase activity. *Proc. Natl. Acad. Sci. USA* **93**, 5489-5494.

Santel, A. and Fuller, M. T. (2001). Control of mitochondrial morphology by a human mitofusin. *J. Cell Sci.* **114**, 867-874.

Simon, J., Bhatnagar, P. L. and Milburn, N. S. (1969). An electron microscope study of changes in mitochondria of flight muscle of ageing houseflies (*Musca domestica*). *J. Insect Physiol.* **15**, 135-140.

Subramanian, K. and Meyer, T. (1997). Calcium-induced restructuring of nuclear envelope and endoplasmic reticulum calcium stores. *Cell* **89**, 963-971.

Terasaki, M., Slater, N. T., Fein, A., Schmidek, A. and Reese, T. S. (1994). Continuous Network of Endoplasmic Reticulum in Cerebellar Purkinje Neurons. *Proc. Natl. Acad. Sci. USA* **91**, 7510-7514.

Tinel, H., Cancela, J. M., Mogami, H., Gerasimenko, J. V., Gerasimenko, O. V., Tepikin, A. V. and Petersen, O. H. (1999). Active mitochondria surrounding the pancreatic acinar granule region prevent spreading of inositol trisphosphate-evoked local cytosolic Ca^{2+} signals. *EMBO J.* **18**, 4999-5008.

Zorov, D. B., Filburn, C. R., Klotz, L. O., Zweier, J. L. and Sollott, S. J. (2000). Reactive oxygen species (ROS)-induced ROS release: A new phenomenon accompanying induction of the mitochondrial permeability transition in cardiac myocytes. *J. Exp. Med* **192**, 1001-1014.